ELSEVIER

Colloids and Surfaces
A: Physicochemical and Engineering Aspects 135 (1998) 63–75

COLLOIDS AND SURFACES A

Poly(ethylene oxide) adsorption onto chemically etched silicates by Brewster angle reflectivity

Zengli Fu, Maria M. Santore *

Department of Chemical Engineering, Polymer Interface center, 111 Research Drive, Lehigh University, Bethlehem, PA 18015, USA

Received 7 April 1997; accepted 2 July 1997

Abstract

A new approach to near-Brewster optical reflectivity measurements is described, implementing internal reflection optics and scanning angle capabilities. The method is then employed to characterize chemically etched layers on soda-lime glass, and study poly(ethylene oxide) (PEO) adsorption from aqueous solution on the silica surface of soda-lime glass. Adsorption isotherms for several narrow molecular weight PEO samples demonstrate that the plateau of the isotherm extends to dilute concentrations, at least as low as 0.01 ppm. Adsorption kinetic measurements revealed transport-limited behavior and facilitated a determination of the free solution diffusion coefficient of PEO. Diffusivity results were in excellent agreement with the literature. © 1998 Elsevier Science B.V.

Keywords: Adsorption isotherm; Brewster angle reflectivity; Diffusion; Glass surface layer; Mass-transport controlled kinetics; Soda-lime glass

1. Introduction

Adsorption of polymers from solution onto solid surfaces occurs in many applications such as the stability control of dispersions, surface modification for adhesion or lubrication, biocompatibilization, and the formation of layered structures for sensor devices. Adsorption kinetics are of great importance to the control of surface layer compositions, especially for cases with competitive adsorption and exchange processes.

Several different techniques have been used to directly measure surface layers. Among them, ellipsometry [1–5], optical reflectivity [6–12], attenuated total reflection infrared spectroscopy (ATR-FTIR) [13–18], total internal reflectance fluorescence (TIRF) [10–23], and streaming potential measurements in capillary flow [24] dominate the literature. Every method, when used alone, is limited in its ability to distinguish competing surface species. Even FTIR is restricted to particular substrates and polymer–solvent systems. Our primary motivation here has been to find a mass-sensitive technique to supplement TIRF studies of fluorescently tagged populations [21] on optically transparent surfaces such as silicate glass. The reflectivity method developed by Dijt et al. [6] to measure polymer adsorption on oxide-coated silicon substrates can directly detect the adsorbed amount, with the signal nearly independent of the polymer layer density. However, the use of an optically nontransparent silicon substrate limits the utility of this approach for comparison with TIRF.

* Corresponding author.

0927-7757/98/$19.00 © 1998 Elsevier Science B.V. All rights reserved.
PII S0927-7757(97)00218-5

The Brewster angle reflectivity method, based on refractive index, can be implemented in internal reflection inside glass substrates, making it possible to conduct adsorption reflectivity experiments parallel with TIRF studies. Although Brewster angle reflectometers with angle scanning capability have been used on pure silica [10,25] or high refractive index glass substrates [11], we know of no reflectivity study of polymer adsorption on silicate glass on which a surface film exists [26–31]. This film potentially complicates the optical calibration.

This paper describes our novel approach to optical reflectivity measurements of polymer adsorption on substrates with surfaces optically different than the bulk substrate material. Calculations are presented to motivate the subsequent interpretation of experimental data. A description of the instrument is provided, and our calibration methods discussed. Then, results are shown to evidence the presence of silica-like surface layers on soda-lime glass for surface treatments relevant to our adsorption studies. Finally, poly(ethylene oxide) (PEO) adsorption isotherms and kinetic data are presented and interpreted in the context of transport limited adsorption.

2. Brewster angle reflectivity at a glass–solution interface

It has been recognized [26–31] that, even without adsorbed polymers, a surface layer usually occurs on silicate glass as a result of chemical treatment (such as the acid as used in our precleaning process), by the contact with water [28,29], or even atmospheric moisture [30]. Leaching of alkali ions and the hydration of the silica are the primary reasons for the formation of the surface layer [26,28,29], which usually has a composition and refractive index approaching those of pure silica [27,30]. Therefore, an interfacial model with at least two layers (one for the adsorbed polymer layer, and the other for the glass surface layer) should be used to predict the reflectivity of polymers adsorbing on silicate glass.

In this work, both the glass surface and the polymer layer are assumed to be homogeneous, i.e. adequately described by a single refractive index for each. In reality there is nonuniform distribution of concentration (and optical density) across each layer; however, the two-layer model is sufficient because the glass surface layer and the adsorbed polymer are much thinner than the wavelength of light. Our numerical calculations have shown that an adsorbed step-function layer will have the same near-Brewster-angle reflectivity as a layer with a complex profile when the total interfacial mass is less then 1 mg/m^2 and the thickness is less than 15 nm (here we modeled the complex profile using 10 internal sublayers of varied refractive index [32]).

The two-layer model is illustrated by Fig. 1, where n_g, n_f, n_p and n_s, represent the refractive indices of the glass, the glass surface layer, the adsorbed polymer layer and the polymer solution, respectively; and d_f and d_p represent the thickness of surface layer and polymer layer. The reflectivity coefficient, r_{ab}, of p-polarized light incident on a sharp interface separating two media with refractive indices n_a and n_b is given by the Fresnel equation:

$$r_{ab} = \frac{n_b \cos\theta_a - n_a \cos\theta_b}{n_b \cos\theta_a + n_a \cos\theta_b}, \quad (1)$$

where the incident angle, θ_a, and the transmitted angle, θ_b, are related by Snell's law: $n_a \sin\theta_a = n_b \sin\theta_b$. In Eq. (1), r_{ab} vanishes at the Brewster angle, θ_B, $=\tan^{-1}(n_s/n_g)$ for a perfect glass-solution interface. The reflectivity, R_p, is defined as the intensity ratio of the reflected light to the incident light, I/I_0, and is given by $|r_{ab}|^2$ (the square of the complex modulus of r_{ab}). An interfacial layer is

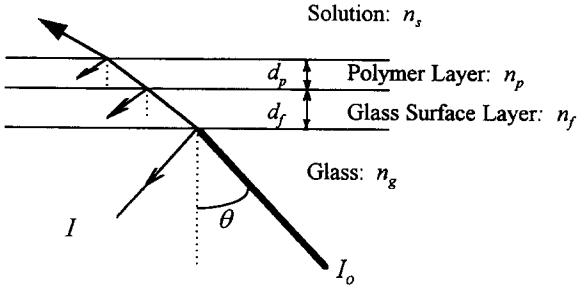

Fig. 1. Brewster angle reflectivity at a glass–solution interface containing two thin layers: an alkali-leached/hydrated surface layer and an adsorbed polymer layer.

easily detected near θ_B, because R_p will change significantly upon adsorption.

The angular-dependent reflectivity, $R_p(\theta)$, from an interface with a single step-function layer is given by [33]

$$R_p = \left| \frac{r_{gj} + r_{js}\, e^{-i2\beta_j}}{1 + r_{gj} r_{js}\, e^{-i2\beta_j}} \right|^2, \quad (2)$$

where r is given by Eq. (1), the subscript j refers to the thin layer at the glass–solution interface; g and s refer to glass and solution, respectively. For two interfacial layers, j and k, the reflectivity for p-polarized light is

$$R_p = \left| \frac{(r_{gj} + r_{jk}\, e^{-i2\beta_j}) + (r_{gj} r_{jk} + e^{-i2\beta_j}) r_{ks}\, e^{-i2\beta_k}}{(1 + r_{sj} r_{jk}\, e^{-i2\beta_j}) + (r_{jk} + r_{gj}\, e^{-i2\beta_j}) r_{ks}\, e^{-i2\beta_k}} \right|^2, \quad (3)$$

where β_j is the layer phase thickness:

$$\beta_j = \frac{2\pi d_j n_j}{\lambda} \cos\theta_j, \quad (4)$$

and λ is the wavelength. For more layers, the Abeles matrix method can be used [33].

The adsorbed amount of polymer, Γ, is related to n_p and d_p through

$$\Gamma = \frac{(n_p - n_s) d_p}{dn_p/dc}, \quad (5)$$

where $dn_p/dc = 0.134$ ($g^{-1}cm^3$) for PEO at $\lambda = 633$ nm [34]. c is the polymer concentration in g/cm^3.

When the phase thickness of the surface layer is much smaller than the polymer layer, (i.e. $\beta_f \ll \beta_p < 1$), Eq. (3) reduces to Eq. (2). Therefore, the decision to include the glass surface layer in the model depends on how the 'optical' thickness of the surface layer compares with that of the adsorbed polymer. Other investigators using Brewster angle reflectivity on silicate glass substrates neglected the surface layer, for example, polystyrene latex deposition on glass [35], because the polymer layer was thick relative to the glass surface layer. PEO layers adsorbed on silicate glass, however, rarely exceed 15 nm in thickness and the local refractive index inside these layers is close to water. PEO layers are, therefore, optically thin and the glass surface layer should not be neglected. To quantitatively measure PEO adsorption, the glass surface layer must be first characterized.

These considerations motivated a thorough numerical analysis, using optical parameters approaching experimental reality, of the physics anticipated for PEO adsorption on silicate glass.

In Fig. 2, R_p is plotted near θ_B as a function of incident angle, θ, using Eq. (2) or Eq. (3). Adsorption of a 0.4 a-mg/m^2 PEO layer at a sharp glass–water interface (curves *i* and *ii* represent before and after the adsorption, respectively) is compared with the same PEO layer on a glass substrate with a chemically altered glass surface layer 13 nm thick (curves *iii* and *iv*). The reflectivity curves generally possesses a parabolic dependence on incident angle. Fig. 2 shows that the presence of interfacial layer(s) shifts the curve upwards. If the layer phase thickness (β) is sufficiently small (as for the case of adsorbed PEO) there is no significant shift of θ_{min}, the angular position for the minimum R_p (note θ_B, the Brewster angle, always refers to the θ_{min} of the perfect interface

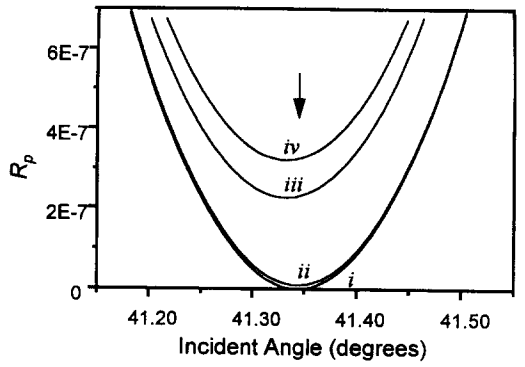

Fig. 2. Reflectivity as a function of incident angle at a glass–water interface. Curve *i*, sharp glass–water interface without surface layer or adsorbed polymer layer; curve *ii*, 0.4 mg/m^2 PEO adsorbed at a sharp glass–water interface; curve *iii*, a surface layer on glass ($d_f = 13$ nm); and curve *iv*, 0.4 mg/m^2 PEO adsorbed on the top of the surface layer. The refractive indices used in these calculations are: $n_g = 1.515$ (glass), $n_f = 1.490$ (surface layer), $n_p = 1.36$ (adsorbed PEO layer), and $n_s = 1.333$ (water) for $\lambda = 633$ nm. The arrow indicates the Brewster angle (θ_B) for the sharp interface (in curve *i*).

without additional layers). However, if β becomes larger (as for the case of glass surface layer), we see a shift of θ_{min}. These observations indicate that for thick layers, two degrees of information are available from the angular scans: the upwards shift of R_p and the angular shift of θ_{min}. For thin layers, there is only one degree of information: the upwards shift of R_p. This finding guided our experimental protocol. Angular scanning measurements facilitated a characterization of the glass surface layer (resulting in n_f and d_f), and experiments at a fixed near-Brewster incident angle measured PEO adsorption kinetics (giving the adsorbed amount as a function of time). Also in Fig. 2, the presence of a glass surface layer enhances the change of R_p during PEO adsorption, an advantage for measurements of PEO adsorption.

Fig. 3(a) and (b) show R_p and $R_p^{1/2}$ at fixed angle, near θ_B, as a function of adsorbed amount, Γ (between 0 and 2 mg/m^2). Here, the layer thickness is increased at fixed n_p as the coverage of PEO is increased. Glass substrates without a surface layer and with surface layers of two different phase thicknesses (β) are shown. The reflectivity is calculated both at θ_{min} and $\theta_{min}\pm0.02°$. R_p is found not to be significantly affected by small deviations in the angular alignment ($\theta_{min}\pm0.02°$) (our instrumental precision is higher than this). The R_p versus Γ dependence in Fig. 3(a) is roughly parabolic, as shown by the rescaling of $\Gamma(R_p^{1/2})$ in Fig. 3(b). The only exception in Fig. 3(b) is the case without the surface layer at angles deviating from θ_B. This observation agrees with the theoretical analysis by Schaaf et al. [10] based on Abeles' 'method of integrals' [36] for the reflectivity calculations. They showed that for any thin layer, when $[n_f(z)-n_s]\ll n_s$, then $R_p(\theta_B)\propto\{\int[n_f(z)-n_s]\,dz\}^2$, where z is the direction normal to the interface and the integral is proportional to the total amount of adsorbed polymer. Our numerical calculations, however, reveal the details of the reflectivity behavior for the thin layers — the slopes of $R_p^{1/2}(\Gamma)$ curves are practically independent of the glass surface layer's optical thickness (β_f) for a constant polymer layer density (n_p), and for glass surface layers that are relevant to this investigation. There

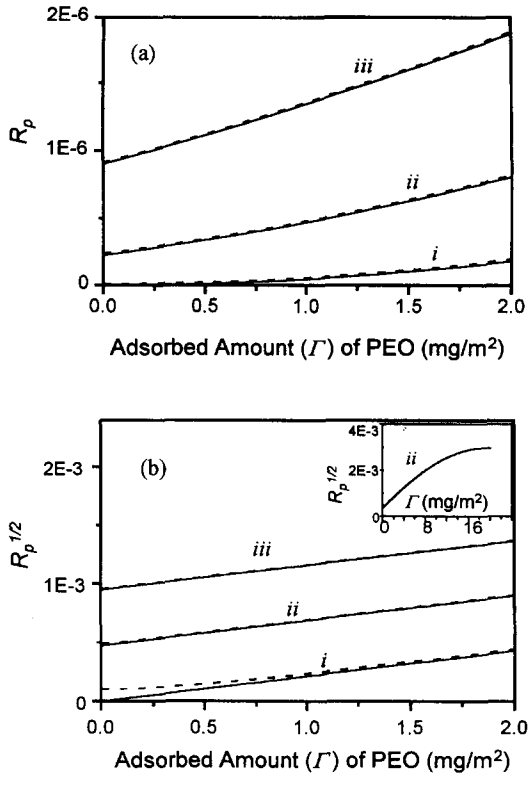

Fig. 3. (a) Reflectivity (R_p); and (b) square root of the reflectivity ($R_p^{1/2}$) at θ_{min} (solid lines) and $\theta_{min}\pm0.02°$ (dashed lines) as a function of adsorbed amount (Γ) for PEO layers (of fixed refractive index) on a glass without a surface layer (curves *i*), and on top of surface layers: (curves *ii*) $n_f=1.490$, $d_f=13$ nm; (curves *iii*) $n_f=1.450$, $d_f=13$ nm. n_g, n_p, and n_s are the same as in Fig. 2. Inset curve in (b) extends the range of curve *ii*.

is, however, a slight dependence of $R_p^{1/2}(\Gamma)$ slope on n_p, to be discussed below. The inset curve in Fig. 3(b) shows $R_p^{1/2}(\Gamma)$ up to 20 mg/m^2 of coverage, illustrating the linear proportionality up to about 8 mg/m^2.

Fig. 4 shows the slope of $R_p^{1/2}(\Gamma)$, $dR_p^{1/2}/d\Gamma$, in the linear range as a function of PEO layer density or average PEO mass fraction (the quantity $dR_p^{1/2}/d\Gamma$ is essentially the calibration constant of our experiments). The y-axis on the right side is scaled as the relative change of $dR_p^{1/2}/d\Gamma$, normalized at $n_p=1.36$, corresponding to a PEO layer density of 20% in aqueous solution. The x-axes also show the average refractive index, n_p, corresponding to each density, obtained via $dn_p/dc=0.134$ for PEO in water. The third x-axis

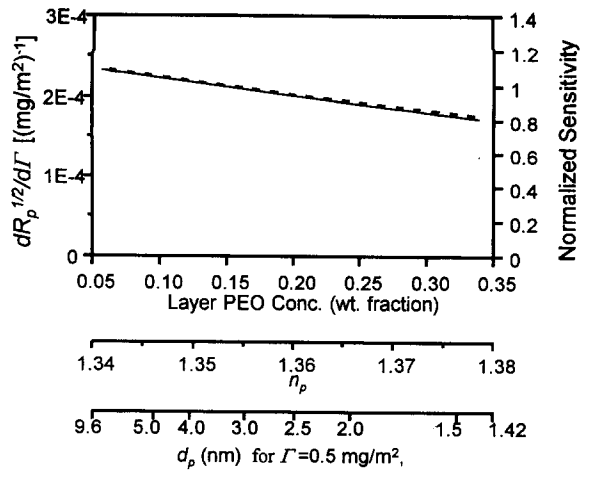

Fig. 4. Adsorption signal sensitivity, $dR_p^{1/2}/d\Gamma$, dependence on the PEO layer density. Solid line is at θ_{min}; dashed lines indicate $\theta_{min} \pm 0.02°$.

shows the corresponding layer thickness (d_p) for an adsorbed PEO layer with 0.5 mg/m^2. The calculation in Fig. 4 employs a glass surface layer ($n_f = 1.490$, $d_f = 13$ nm) and gives results for θ_{min}, and $\theta_{min} \pm 0.02°$. The results are generally independent of the surface layer thickness [as shown by Fig. 3(b)]. The significance of Fig. 4 is that the adsorption signal sensitivity, $dR_p^{1/2}/d\Gamma$, is only a weak function of polymer layer density. For the same adsorbed amount, a dense layer will give slightly smaller reflectivity signal than a fluffy layer. If the average PEO layer density is 20%, a change in density from 20 to 10% or to 30% will cause only a 10% change in the reflectivity signal.

In summary, these calculations demonstrate that for a fixed near Brewster angle reflectivity measurement of adsorbed PEO, $R_p^{1/2}(\Gamma)$ is linear in Γ over a substantial range of Γ, and that this relationship is not affected by the optical nature of the glass surface layer over the experimentally accessible range of such glass surfaces. In addition, small deviations in the incident angle from θ_B (or θ_{min}) do not affect R_p significantly. To first order, the adsorption signal sensitivity does not change much when the polymer layer's density experiences limited variations.

3. Experimental

3.1. Materials

Soda-lime glass microscope slides (FISHER*finest*) were used as the adsorption substrate. The bulk glass was reported by the manufacturer (Erie Scientific) to have the following composition: SiO_2, 72.1%; Na_2O, 14.0%; CaO, 7.3%; MgO 3.8%; Fe_2O_3/FeO, K_2O, Al_2O_3 <2.0% each. A slide was placed in the adsorption flow cell which was then filled with concentrated sulfuric acid to treat the glass surface in situ for 15 h. ESCA studies revealed that the glass surface composition after this acid treatment was primarily SiO_2, while an untreated slide's atomic surface composition was consistent with the manufacturer's report [37]. After the sulfuric acid treatment, the cell was flushed with copious amounts of DI (deionized) water. The cell was then flushed with 0.005 N NaOH for 10 min, followed by 0.5 M H_2SO_4 for 10 min, and DI water to neutralize the cell and the surface. The surface was then ready for the PEO adsorption experiment. After an adsorption experiment, the same base–acid cleaning cycle was used to remove the adsorbed PEO, and to regenerate the surface. This cleaning procedure was found to give reproducible PEO adsorption kinetics and was therefore used for many of the kinetic experiments that were conducted in series. In situ surface regeneration facilitated repeated use of a single cell calibration and avoided unnecessary optical realignments.

The following monodisperse PEO samples (from Polymer Laboratories Inc.) were used: MW 32.6K ($M_w/M_n = 1.03$), MW 120K ($M_w/M_n = 1.02$), MW 448K ($M_w/M_n = 1.07$) and MW 963K ($M_w/M_n = 1.1$).

3.2. The adsorption flow cell

In order to conduct the adsorption under controlled shear-flow conditions, we employed a thin rectangular flow channel with dimensions $0.13 \times 1.0 \times 4.0$ cm. An entrance region (per the design of Shibata and Lenhoff [38]) minimized the entrance effects. Liquid was pumped through the channel between the glass surface and the wall of

the black Teflon base. Adsorption under shear flow conditions occurred on the glass surface and the adsorption kinetics at the center of the surface were monitored using a laser beam. A syringe pump maintained flow for kinetic studies while a peristaltic pump was used for slow equilibration experiments.

3.3. The scanning angle reflectometer

Two different types of scanning Brewster-angle reflectometers appear in the literature. Schaaf and coworkers [10,25] conducted the angular scans either by moving the laser and photo-detector relative to the sample, or by rotating the sample and moving the detector with respect to the laser. This set-up gave good quality scan data, but took a significant time to complete each scan, thereby limiting the utility for fast kinetic studies. Leemakers and Gast [11] developed a dynamic scanning angle reflectometer using a cylindrical lens to focus the laser beam on the interface and simultaneously measuring the angular dependence of R_p with an array detector. This provided rapid data acquisition; however, the quality appeared to be reduced because the incident intensity was decreased by dispersing the laser beam to access multiple angles.

We constructed a modified version of the Schaaf's scanning angle reflectometer, shown in Fig. 5. The light source is a 2.0 mW helium–neon laser (Uniphase Model no. 1122P, $\lambda = 632.8$ nm). Its beam passes through a Glan–Thompson polarizer, and then is directed by a steering mirror to the sample cell which employs a BK-7 glass prism wave guide. The reflected light beam passes out of the prism, through a pinhole (used only during fixed angle kinetic measurements), through a second polarizer, and to the photodiode detector.

For scanning angle measurements, the mirror is manually rotated, resulting in a change of the incident angle and a small movement of the beam along the interface. The reflected beam is detected on an array detector (Alton Instrument Corp., Model LS-2000). All of the beam's movements were proven to be geometrically linear, because the mirror rotates through a very small angular range (usually less than 1°). For each single angular position, the reflected beam appears on the detector array as a gaussian profile. When the incident angle is changed, the beam peak intensities and positions are recorded, thus giving the angle scan envelope (see Fig. 6). Detection of a single beam profile usually takes 0.05 s, enabling a full angle scan to be finished within 10 s for no less than 50 angular positions. The total detecting area of the interface, for the scanning angle measurement, is illustrated by the circles on the upper part of Fig. 5. For a 0.5° change in the incident angle, there is a 1.3 mm shift of the center of the beam spot, while the beam has a diameter of about 0.7 mm.

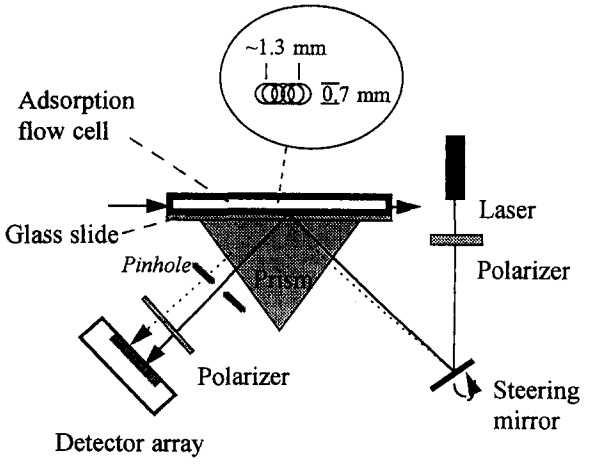

Fig. 5. Schematic of the reflectometer apparatus.

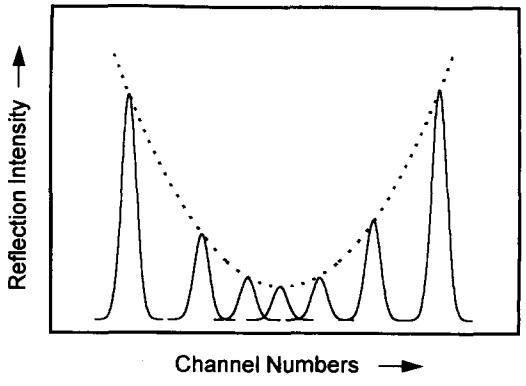

Fig. 6. Schematic illustration of the original angle scan data: the peak intensity and angular position for each gaussian beam profile were taken as a data point of the reflectivity scan.

For kinetic studies at fixed angle, we preferred to used a single-point photodiode detector instead of the photodiode array. The former has a wider detection window (2.5 × 2.5 mm) providing a larger tolerance to the alignment shifts from thermal drift during long runs.

3.4. Calibration of angle scan reflectivity data

The reflectivity signal (in counts) on the y-axis and the angular position (in channel numbers of the detector array) on the x-axis are the raw data that need to be converted to R_p, and θ, respectively. The x-axis calibration employed several salt solutions of known refractive indices, n_s, to find the corresponding Brewster angle positions. The channel numbers were thereby converted into θ_Bs which were calculated from the refractive index pairs, n_g and n_s. The scale of the x-axis was double-checked by converting the change in detector channel numbers from 2° of mirror rotation into the real incident-angle change in the glass substrate (which was calculated using geometric optics). This second check was in excellent agreement with the salt solution method. After the x-axis calibration, we fitted the angle-scan curves to Eq. (3) to convert intensity counts to R_p on the y-axis. For all of the reflectivity data, a very small amount of baseline from background light and scattering was subtracted from the original reflectivity signal.

Fig. 7 shows the calibration results, and demonstrates the quality of the angle-scan data. The glass surface used in this calibration was pre-treated by NaOH solution and most of the surface layer had been removed (as discussed in the next section) so that θ_{min} was essentially equal to θ_B. The agreement between the data and Eq. (3) showed that the interface was sharp and only a very thin surface layer remained.

4. Results and discussion

4.1. Glass surface layer characterization and PEO adsorbed amount

Scanning angle reflectivity data for a glass/water interface with and without an adsorbed PEO layer are shown in Fig. 8. Curve *i* is for the surface after the full cleaning procedure and curve *ii* was measured after the adsorption of PEO (MW 448K) from DI water. Curve *i* contains a minimum of nonzero intensity. Since the baseline signal was already subtracted, two reasons remain for the nonzero minimum: (1) surface roughness; or (2) the glass surface layer. We measured the surface roughness by AFM after the cleaning procedure and found a r.m.s. roughness of 0.6 nm, in agreement with ellipsometric [31] and X-ray reflectivity [27] examinations of similar types of

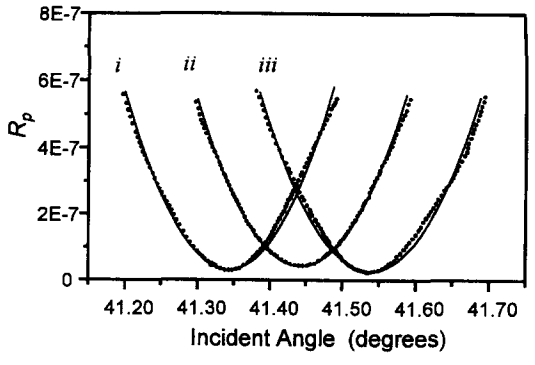

Fig. 7. Calibration of reflection angle and R_p via angular scans with (*i*) DI water (n_s = 1.3330); (*ii*) 2.44% NaCl solution (n_s = 1.3374); (*iii*) 4.76% NaCl solution (n_s = 1.3418); and the glass substrate (n_g = 1.515). Data (dots) are compared with Eq. (3) (lines).

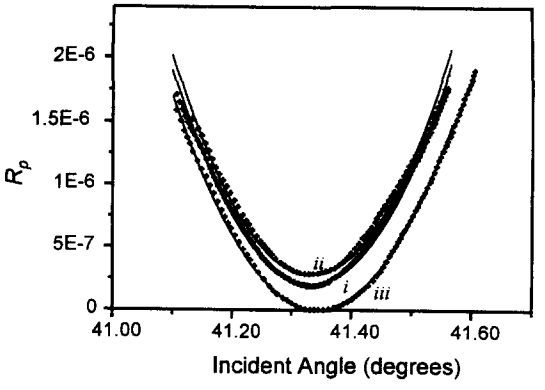

Fig. 8. Scanning angle reflectivity for (*i*) precleaned glass surface (with surface layer) in contact with DI water, (*ii*) adsorbed PEO (MW 448K) layer on the surface layer, and (*iii*) after the removal of PEO layer and surface layer by 0.005 N NaOH solution. Data (dots) are compared with calculations (lines).

commercial soda-lime glass surfaces. Roughness levels on this order are too thin to explain the magnitude of curve *i* in Fig. 8. In addition, more severe scattering would be expected to give nonparabolic intensity profile. Therefore a chemically distinct surface region is the best explanation.

After PEO adsorption, the surface was exposured to flowing 0.005 N NaOH solution for several hours beyond that required to remove the PEO layer. This caused a decrease in the reflectivity, finally to a minimum value of zero at θ_B, as illustrated by curve *iii* in Fig. 8. The evolution occurring during the basic wash step was also measured at fixed θ_B in Fig. 9. This experiment evidenced the existence of the surface layer. The dissolution of such layers (alkali-leached hydrated SiO_2) in basic solutions is well documented [26,28,29,39]. The final glass–solution interface (in curve *iii* of Fig. 8) must be very sharp, because the reflectivity is well described by Eq. (1).

A slight increase of R_p was always seen after switching from 0.005 N NaOH back to DI water, as illustrated at the end of the experiment in Fig. 9. This may result from the re-association of protons (H^+) back to the surface silanol groups as the pH drops, and the formation of a thin surface layer with a different refractive index from that of bulk glass (note that all surface silanols should be dissociated above pH ~ 11). The change of the bulk–solution refractive index (from DI water to 0.005 N NaOH solution or vice versa) is sufficiently small so that there is no angular shift of the curve. The signal increase in Fig. 9 corresponds only to

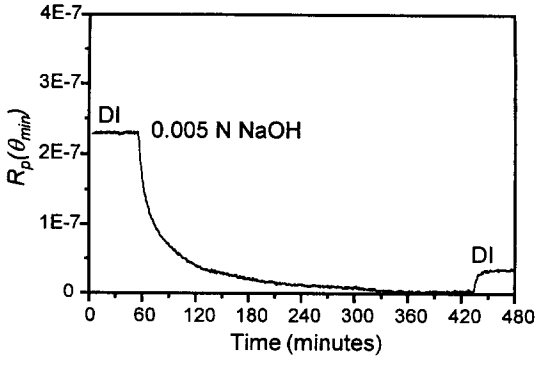

Fig. 9. Dissolution kinetics of glass surface layer on exposure to flowing of 0.005 N NaOH solution.

an upward shift of $R_p(\theta)$. This observation illustrates how sensitive the Brewster angle reflectivity is to thin layers at an interface.

We fitted the scanning angle reflectivity data in Fig. 8 using Eqs. (1)–(3), yielding the following results. The glass surface layer (after concentrated H_2SO_4 treatment for 15 h) was described by $n_f = 1.49$ and $d_f = 13$ nm. The adsorbed PEO layer (MW = 448K) was described by $n_p = 1.36$, $d_p = 2.5$ nm, giving $\Gamma = 0.5$ mg/m^2. We are confident in our measurements of the glass surface layer properties because independent measurement of θ_{min} and $R_p(\theta_{min})$ allowed independent determination of n_f and d_f. In fitting the polymer layer, however, we assumed a mass fraction in the layer of 20% PEO (based on neutron reflectivity measurements [40]), corresponding to $n_p = 1.36$. The value of $d_p = 2.5$ nm was then determined from the fit to the experimental data. As discussed in the calculation section, we cannot be exactly sure of the layer thickness for PEO because we cannot directly measure n_p; however, our confidence in Γ is within 10% error.

Concern about the durability of the underlying alkali-leached hydrated surface layer (during the PEO adsorption studies) motivated closer scrutiny of the processes for glass surface layer formation and dissolution. Surface leaching to form the 'glass surface layer' is an ion exchange process [28]:

$$Na^+(g) + 2H_2O \leftrightarrow H_3O^+(g) + Na^+ + OH^-, \quad (6)$$

where g is the glass. It has been found that concentrated strong acids (HCl and H_2SO_4 above 1 M) attack soda-lime glass more rapidly than dilute acids or neutral solutions [41]. Following the initial rapid attack, a subsequent reduction of the attack rate results from slow ion-diffusion through the surface layer which protects the bulk glass.

The dissolution of the surface layer occurs by several successive reactions that break up the silicon-oxygen network [28]:

$$H_2O + Si{-}O{-}Si \leftrightarrow SiOH + HOSi \leftrightarrow H_4SiO_4. \quad (7)$$

The rate for dissolution in Eq. (7) at pH values near or moderately below 7 is very slow [26]. This means that during PEO adsorption, the glass surface layer is durable. Indeed, our reflectivity experiments also showed that the R_p can be maintained

fairly stable for several days when the surface is in contact with neutral aqueous solutions. At longer times and at warmish room temperatures, we frequently found a gradual increase of R_p, indicating an increase of the glass surface layer phase thickness (β_f). This suggests that leaching occurs slightly more rapidly than dissolution at such conditions.

The dissolution rate in Eq. (7) becomes rapid in basic solutions above pH 9 [26] in accordance with Fig. 9, where the surface layer dissolution in 0.005 N NaOH solution is initially rapid, and takes about 6 h for complete removal (at a wall shear rate of 7.2 s^{-1}). We did not see a significant amount of glass surface layer remaining at the end of the experiment, indicating that dissolution kinetics dominates ion exchange in basic solutions, an observation consistent with previous studies [26].

In summary, in neutral or dilute acid solutions, the glass surface layer formed by our H_2SO_4 cleaning process is sufficiently stable for PEO adsorption studies. This surface layer, however, can almost be completely removed by contact with basic solution for several hours, leaving a sharp glass–solution interface which can be used to calibrate the instrument. We therefore employed fixed angle (single point reflectivity) measurements for the adsorption isotherm and kinetics studies. R_p was converted to Γ based on the surface layer characterization result and the assumption of an average PEO layer density (we used $n_p = 1.36$, corresponding to 20% of PEO chain in the layer).

4.2. Adsorption isotherms

In general, a quantitative understanding of adsorption kinetics requires knowledge of the adsorption equilibria, because the local concentration in the fluid element near the surface in equilibrium with the instantaneous adsorbed amount defines the maximum driving force for diffusion of the adsorbing species from the bulk solution to the surface. Without adsorption isotherm data at very low concentrations, kinetic treatments often assumed a Langmuir-shaped isotherm [42] or a linear equilibrium relation [38]. It is extremely difficult to accurately measure isotherms below several ppm of bulk concentration for colloidal substrates; however, the use of an adsorption flow cell, planar substrates and techniques such as optical reflectivity to measure the adsorbed amount make such measurements possible.

Adsorption isotherms for monodisperse PEO samples from DI water on silica glass substrates with surface layers like those previously described are shown in Fig. 10. Equilibrium bulk concentrations (C_{eq}) as low as 0.01 ppm were achieved. At these extremely dilute concentrations, the surface coverage was similar to that at higher concentrations. This indicates the high affinity nature of PEO adsorption on silica. Notably, the adsorption kinetics at the most dilute concentrations were extremely slow, requiring more than 24 h to reach equilibrium for 0.01 ppm. This time should be compared to less than 1 min with 100 ppm PEO. High affinity isotherms for polymer adsorption have been predicted using Scheutjens–Fleer theory, and the plateau of the isotherm was predicted to extend down to $C_{eq} = 10^{-4}$ ppm [24]. These low concentrations are essentially unattainable in real experiments. To our knowledge, $C_{eq} = 0.01$ ppm is the lowest free solution concentration studied, and it is negligibly low compared with the bulk concentrations used in most kinetic studies. This means that if local equilibria were maintained during

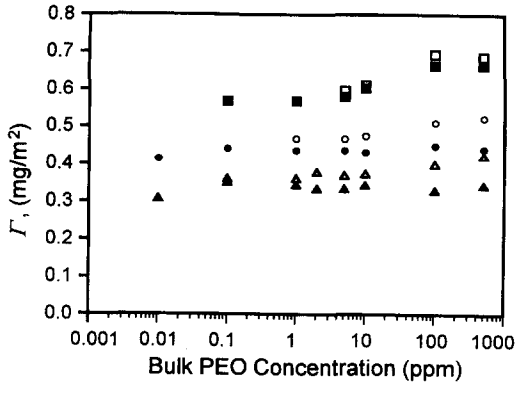

Fig. 10. Adsorption isotherms of PEO from DI water: (Δ,▲) MW 32 600; (○, ●) MW 120 000; (□, ■) MW 963 000. Hollow symbols represent the maximum adsorbed amounts on surface during contact with polymer solutions. Solid symbols represent the amounts retained after rinsing the layers with DI water for 25 min.

adsorption or desorption, the free fluid nearest the surface would contain essentially no polymer.

Fig. 10 also shows the adsorbed amounts after rinsing the adsorbed layers with DI water (represented by the solid symbols; note that at places where only solid symbols are seen, no changes were found after rinsing). We usually observed a small amount of desorption within 15 min of flowing solvent, followed by a signal that was flat for several hours, indicating strong layer retention. The exceptions were at the lowest bulk concentrations. The initial signal drop on rinsing suggests that there is a small fraction of loosely bound chains in the layer, which is smaller for higher MW samples.

In Fig. 10, the plateau coverages of 0.3–0.7 mg/m^2 are similar to those previously reported for PEO on silica in this pH and molecular weight range [6,43,44]. Small differences in absolute coverage (order of 0.1 mg/m^2) between our work and the literature are attributed to the different silica surfaces employed in different laboratories. In addition, the absolute coverage levels reported in Fig. 10 are in qualitative agreement with other methods of determining PEO adsorption on silica, for example, isotherms on silica particles requiring separation of serum and sediment [22]. Isotherms on silica particles cannot be employed as a test of the accuracy of the reflectivity method, because the particulate method is not sufficiently precise (error from determining serum polymer concentration propagates to the calculation of the adsorbed amount) and because the particle surface may be different from the planar microscope slide, introducing real differences in coverage. The accuracy of the coverages reported in Fig. 10 is upheld by the measurements of the diffusion coefficients (in the next section) which required knowledge of the absolute amount.

In the range of molecular weights examined (from 32 600 to 963 000), the plateau adsorbed amounts were found to increase with the PEO molecular weight. These results are in qualitative agreement with the Scheutjens–Fleer theory which predicts that the molecular weight dependence of the adsorbed amount is stronger in near-Θ solvents (χ close to 0.5) and becomes weaker in a good solvent (χ close to 0) [45]. For PEO in water, χ is about 0.41–0.45 [46,47], indicating near-Θ conditions. A similar influence of molecular weight on coverage (for this range of molecular weights) was also found by Dijt et al. [6].

4.3. Kinetics of PEO adsorption

Fig. 11 demonstrates the wall shear rate sensitivity of the PEO (MW=32.6K) adsorption rate from 5 ppm solution onto silica glass. The remarkable feature of these adsorption traces is the nearly constant adsorption rates all the way to full coverage. Only initially do the traces show upward curvature. Parallel kinetic measurements using total internal reflectance fluorescence (TIRF) with a labeled version of the same molecular weight PEO [48] showed a linear signal rise, proportional to adsorbed amount, over the entire adsorption process. We believe that Γ is actually linear with time as shown by TIRF and the slight curvature in the early stages of the reflectivity results from variations in layer density. If the first chains to adsorb form a flat dense layer that, with the adsorption of new chains, becomes fluffy and less dense, then $dR^{1/2}/d\Gamma$ in Fig. 4 will increase. This means that, during changes in layer density, the adsorption traces will be concave up.

In studies determining factors affecting the adsorption rates, we were primarily concerned with the overall or average rate in curves like those in Fig. 11. The average rate was taken as the slope

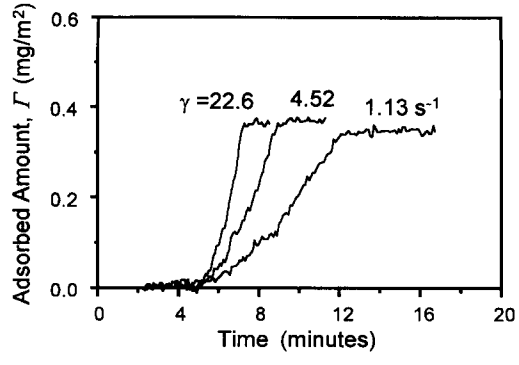

Fig. 11. Kinetics of PEO adsorption from DI water at varied wall shear rates on silica glass surface measured by Brewster angle reflectivity. PEO, MW 32.6K. Bulk solution, 5 ppm in DI water.

of the linear regression of the main part of the curve between 10 and 90% of surface coverage.

Fig. 12 illustrates the 1/3 power law dependence of the adsorption rate on wall shear rate, and the linear dependence of the adsorption rate on concentration for concentrations below 15 ppm. Both functionalities are indicative of mass-transport limited kinetics, the maximum possible adsorption rate. The Leveque equation [49] describing mass transport limited adsorption is the pseudo-steady-state solution of the diffusion convection equation:

$$\frac{d\Gamma}{dt} = 0.538\left(\frac{\gamma}{L}\right)^{1/3} D^{2/3} C_b. \quad (8)$$

Here, C_b is the bulk solution concentration, L is the lateral distance from the cell entrance to the point of observation, and D is the diffusion coefficient of the adsorbing species (free coils or clusters) in bulk solution. Eq. (8) holds once the pseudo-steady state concentration gradient near the surface has been established. Shibata and Lenhoff [38] have shown that this condition is met when the dimensionless time, τ, exceeds unity.

$$\tau = \frac{t}{L^{2/3}/(\gamma^{2/3} D^{1/3})} \quad (9)$$

Eq. (8) also assumes that the surface has an infinite capacity for the adsorbing species. If the surface becomes saturated or the intrinsic adsorption rate slows because of a partially filled surface, then Eq. (8) no longer applies and the adsorption rate slows to zero.

During mass-transport-limited adsorption, the local concentration of polymer in the fluid nearest the surface is vanishingly small, making the dilute concentrations on the x-axis of Fig. 10 relevant, as discussed by Dijt et al. [24]. The fast rate of adsorption and the abrupt saturation of the surface (consistent with the extension of the plateau down to extremely dilute solutions in Fig. 10) suggest that local equilibrium is maintained over the entire adsorption process, and that PEO equilibrates relatively rapidly at the interphase.

When Eq. (8) applies, bulk solution diffusivities can be calculated from experimentally measured adsorption rates. Table 1 summarizes these diffusivities for a variety of PEO molecular weights, with kinetic measurements made at dilute solution conditions of 1–5 ppm. The results compare well with values calculated from the radius of gyration (R_g) from dynamic light scattering (DLS) reported by Cohen Stuart et al. [50]. Here R_g is correlated to the molecular weight via $R_g = 0.0504\ MW^{0.5}$ (nm), and D is calculated from the Stokes–Einstein equation,

$$D = \frac{kT}{6\pi\mu R_H}, \quad (10)$$

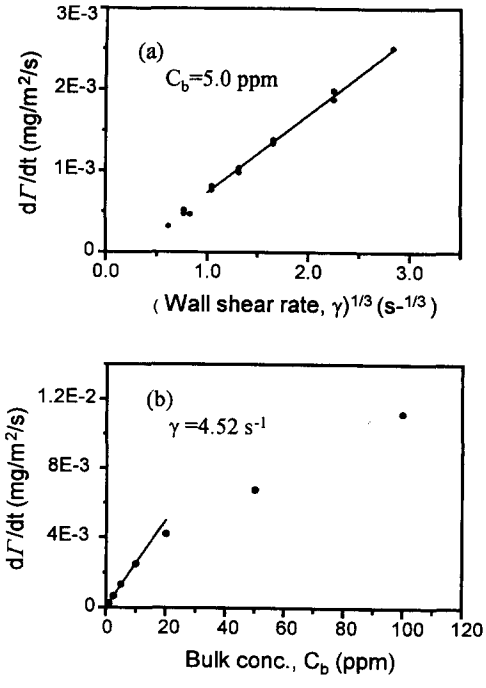

Fig. 12. Rate of PEO (MW 32.6K) adsorption from DI water (a) as a function of (wall shear rate)$^{1/3}$, and (b) as a function of bulk PEO concentration.

Table 1
Diffusion coefficients from adsorption kinetics

MW	$[d\Gamma/dt]/C_b \times 10^5$ (cm/s) (at $\gamma = 5.7\ 4s^{-1}$)	$D \times 10^7$ (cm^2/s)	
		Found in this experiment	Reference [45], see text
32 600	3.86	3.48	3.52
120 000	2.54	1.87	1.83
448 000	2.02	1.33	0.91

where k is the Boltzmann constant, T is the absolute temperature, and μ is the viscosity of water. R_H is the hydrodynamic radius of the polymer coil, which is related to R_g for a nondraining model [51] by

$$R_H = 0.676 R_g \quad (11)$$

Other free solution diffusivities for PEO measured by DLS [52,53] or NMR [54] were also found to concur with our data. Because calibration of D from reflectivity data requires the knowledge of the adsorbed amount in Eq. (8), the agreement of our diffusivity values with those in the literature validates the coverage levels reported in Fig. 10.

The apparent nonlinear concentration dependence of the adsorption rate in Fig. 12 occurs because at concentrations exceeding 20 ppm, the surface is saturated before the local concentration gradient reaches its pseudo-steady-state value. (Prior to $\tau = 1$, the concentration gradient is less than the pseudo-steady-state value, giving slower adsorption than the maximum rate.) From Eq. (9), one finds that the characteristic time $\tau = 1$ occurs at a time of 86.7 s, for a PEO sample with a molecular weight of 33K, a wall shear rate of $4.52\ s^{-1}$, and a bulk solution concentration of 20 ppm. However, if adsorption were to occur at the maximum rate from Eq. (8) (which gives $0.007\ mg/m^2/s$ adsorption rate for the above mass-transport condition), then it would require only ~ 50 s to reach a surface coverage of $0.35\ mg/m^2$, the equilibrium value in Fig. 10. Therefore adsorption kinetics from solutions whose concentrations exceed 20 ppm are not described by the Leveque equation. For the range of conditions studied here, however, it is likely that local equilibrium between the surface and free solution is still maintained, since Dijt found that in stagnation point flow (which has a higher mass-transport coefficient than in this case) PEO adsorption rates were mass-transport controlled up to $0.4\ mg/m^2/s$ [6].

5. Conclusions

We presented a new near-Brewster optical reflectivity experiment and calculations showing that, for parameters within our experimental range, the amount of adsorbed polymer was approximately proportional to the square root of reflectivity, independent of any chemically etched surface layers on the glass. Only a slight dependence of the calibration constant on the layer density was found. We then employed the apparatus to characterize acid-etched surface layers and demonstrated the dissolving of these surface layers in basic solution. Adsorption of PEO on silica surface layers was found to be on the order of $0.5\ mg/m^2$, with the adsorbed amount increasing with molecular weight. The shape of the adsorption isotherms was extremely high affinity, with the plateau of the isotherm extending down to solutions as dilute as 0.01 ppm. Adsorption kinetics measured at fixed angle revealed transport-limited behavior. From the adsorption kinetics, free solution diffusivities of PEO coils were calculated and found in excellent agreement with the literature.

Acknowledgment

This work was made possible by grants from Exxon, AT&T, the National Science Foundation (CTS-9209290) and support from Lehigh's Polymer Interfaces center.

References

[1] M. Malmsten, F. Tiberg, Langmuir 9 (1993) 1098.
[2] J.R. Dorgan, M. Stamm, C. Toprakcioglu, R. Jerome, L.J. Fetters, Macromolecules 26 (1993) 5321.
[3] M. Malmsten, J. Colloid Interfacial Sci. 166 (1994) 333.
[4] L. Odberg, S. Sandberg, Langmuir 11 (1995) 2621.
[5] F. Tiberg, M. Landgren, Langmuir 9 (1993) 927.
[6] J.C. Dijt, M.A. Cohen Stuart, J.E. Hofman, G.J. Fleer, Colloids Surf. 51 (1990) 141.
[7] J.C. Dijt, M.A. Cohen Stuart, G.J. Fleer, Macromolecules 27 (1994) 3207.
[8] J.C. Dijt, M.A. Cohen Stuart, G.J. Fleer, Macromolecules 27 (1994) 3219.
[9] J.C. Dijt, M.A. Cohen Stuart, G.J. Fleer, Macromolecules 27 (1994) 3229.
[10] P. Schaaf, P. Dejardin, A. Schmitt, Langmuir 3 (1987) 1131.
[11] F.A.M. Leermakers, A.P. Gast, Macromolecules 24 (1991) 718.

[12] J.R. Charron, R.D. Tilton, J. Phys. Chem. 100 (1996) 3179.
[13] D.J. Kuzmenka, S. Granick, Colloids Surf. 31 (1988) 105.
[14] P. Frantz, S. Granick, Phys. Rev. Lett. 66 (1991) 899.
[15] H.M. Schneider, S. Granick, Macromolecules 25 (1992) 5054.
[16] P. Frantz, S. Granick, Macromolecules 27 (1994) 2553.
[17] P. Frantz, S. Granick, Macromolecules 28 (1995) 6915.
[18] A. Couzis, E. Gulari, Macromolecules 27 (1994) 3580.
[19] B.K. Lok, Y-L. Cheng, C.R. Robertson, J. Colloid Interface Sci. 91 (1983) 87.
[20] C.T. Shibata, A.M. Lenhoff, J. Colloid Interface Sci. 148 (1992) 469.
[21] M.M. Santore, M.S. Kelly, E. Mubarekyan, V.A. Raber, in Surfactant Adsorption and Surface Solubilization, Chapter 11, ACS Symposium Series 615, 1995.
[22] V.A. Rebar, M.M. Santore, Macromolecules 29 (1996) 6262.
[23] V.A. Rebar, M.M. Santore, Macromolecules 29 (1996) 6273.
[24] J.C. Dijt, M.A. Cohen Stuart, G.J. Fleer, Macromolecules 25 (1992) 5416.
[25] L. Heinrich, E.K. Mann, J.C. Voegel, G.J.M. Koper, P. Schaaf, Langmuir 12 (1996) 4857.
[26] R.H. Doremus, Glass Science, 2nd Edition, Chapter 13, Wiley, New York, 1994.
[27] J.M. Grimal, P. Chartier, P. Lehuede, J. Noncryst. Solids 196 (1996) 128.
[28] R.H. Doremus, Y. Mehrotra, W.A. Lanford, C. Burman, J. Mater. Sci. 18 (1983) 612.
[29] W.A. Lanford, K. Davis, P. Lamarche, T. Laursen, R. Groleau, R.H. Doremus, J. Noncryst. Solids 33 (1979) 249.
[30] M. Huppauff, B. Lengeler, J. Appl. Phys. 75 (1994) 785.
[31] J. Hrdina, Thin Solid Films 233 (1993) 50.
[32] Z. Fu, Ph.D. Dessertation, Lehigh University, Bethlehem, PA, 1997.
[33] R.M.A. Azzam, N.M. Bashara, Ellipsometry and Polarized Light, North Holland, Amsterdam, 1989.
[34] W.F. Polik, W. Burchard, Macromolecules 16 (1983) 978.
[35] E.K. Mann, E.A. van der Zeeuw, G.J.M. Koper, P. Schaaf, D. Bedeaux, J. Phys. Chem. 99 (1995) 790.
[36] F. Abeles, Ann. Phys. 5 (1950) 596.
[37] V.A. Rebar, M.M. Santore, J. Colloid Interface Sci. 178 (1996) 29.
[38] C.T. Shibata, A.M. Lenhoff, J. Colloid Interface Sci. 148 (1992) 485.
[39] R.K. Iler, The Chemistry of Silica: Solubility, Polymerization, Colloid and Surface Properties, and Biochemistry, Wiley, New York, 1979.
[40] E.M. Lee, R.K. Thomas, A.R. Rennie, Europhys. Lett. 13 (1990) 135.
[41] R. Wollast, P. Brennet, A. Jelli, Verres Refract. 24 (1970) 251.
[42] Y. Wang, R. Rajagopalan, Macromolecules 28 (1995) 7058.
[43] K.Th. Wild, N. Gutling, H. Maier, Colloids Surf. 18 (1986) 241.
[44] G.P. van der Beek, M.A. Cohen Stuart, Langmuir 7 (1991) 327.
[45] G.J. Fleer, M.A. Cohen Stuart, J.M.H.M. Scheutjens, T. Cosgrove and B. Vincent, Polymers at Interfaces, Chapter 5, Chapman and Hall, London, 1993.
[46] J. Brandrup, E.H. Immergut (Eds.), Polymer Handbook, 3rd edn, Wiley-Interscience, New York, 1988.
[47] E. Edmond, A.G. Ogston, Biochem. J. 109 (1968) 569.
[48] Z. Fu, M.M. Santore, Langmuir, in press.
[49] M.A. Leveque, Ann. Mines 13 (1928) 284.
[50] M.A. Cohen Stuart, F.H.W.H. Waajen, T. Cosgrove, B. Vincent, T.L. Crowley, Macromolecules 17 (1984) 1825.
[51] H. Yamakawa, Modern Theory of Polymer Solutions, Harper and Row, New York, 1971.
[52] W. Brown, Macromolecules 17 (1984) 66.
[53] B.B. Sauer, H. Yu, Macromolecules 22 (1989) 786.
[54] R.A. Waggoner, F.D. Blum, J.C. Lang, Macromolecules 28 (1995) 2658.